Energetic and Topological Analyses of Cooperative σH- and πH-Bonding Interactions

Igor Vorobyov, M. Cecilia Yappert, and Donald B. DuPré*

Department of Chemistry, University of Louisville, Louisville, Kentucky 40292

Received: July 8, 2002; In Final Form: August 31, 2002

A recent high-level ab initio study (*J. Phys. Chem. A* **2002**, *106*, 567) analyzed the formation of cooperative πH- and σH-bonding motifs in MP2/6-311++G(2d,2p)-optimized complexes of either one or two water molecules with ethene, propene, or allyl alcohol. The present study explores energetics and electron density redistributions associated with hydrogen bonding interactions in these clusters. Despite a substantial correlation component in the binding energy, the nonadditive three-body term, a descriptor of cooperative effects, is completely accounted for at the Hartree−Fock level. Natural bond orbital analysis attributes this cooperativity to the nonadditive character of charge-transfer interactions among local bond orbitals. Topological analysis of the electron density performed using Bader's theory of atoms in molecules confirms the closed shell, hydrogen-bonding nature of OH···π interactions and indicates their additional floppiness compared to conventional hydrogen bonds. The extension of these calculations to larger molecular systems validates the formation of a cooperative network of πH and σH bonds between the interfacial region of ceramide and water molecules. The OH···π bond serves to tether a water molecule to the trans double bond of the sphingolipid, extending the hydrophilicity of the interfacial region. This may contribute to the differences in biological activity between ceramide and its saturated counterpart, dihydroceramide.

1. Introduction

The presence of weak, bonding interactions involving unsaturated aliphatic and aromatic systems as proton acceptors, denoted πH bonds, has been demonstrated experimentally in gas and liquid phases as well as in crystal structures.[1] The difference between these interactions and conventional H bonds (denoted here as σH bonds) is a matter of strength and symmetry, not kind. It was recently shown that both πH and σH bonds can participate as full members in the formation of cooperative H-bonding networks.[2]

Relevant to our research is the analysis of σH and πH bonds that could stabilize the structural motifs adopted by the interfacial region of hydrated ceramides (Cers). NMR studies showed two tightly bound water molecules, one of which is likely to be tethered by the OH···π interaction to the trans double bond between carbons 4 and 5 of the sphingoid base.[3] Water molecules are not able to remain in the vicinity of carbons 4 and 5 in the saturated Cer analogue, dihydroceramide (DHCer), because this interaction is eliminated.[3] Interestingly, Cer has been identified as a second messenger in a variety of signaling pathways that mediate cell growth and differentiation, cell cycle arrest, and apoptosis,[4] whereas DHCer is inactive in these processes.[5] The proposed variations in H-bonding interactions exhibited by the two lipids could account for their different biochemical behavior.

Intra- and intermolecular OH···π bonding interactions have been already studied theoretically by a variety of methods ranging from early semiempirical calculations to more recent high level ab initio optimizations using extended basis sets and electron correlation.[2,6−13] The flatness of the potential energy surface in these clusters and the role of the dispersion forces in the binding were emphasized. Strengthening of both OH···π and OH···O interactions in clusters of water oligomers with π systems was also noted.[6−8]

The focus of our previous theoretical study[6] was an assessment of the cooperative enhancement of both OH···π and OH···O interactions in the presence of a second water molecule and the alcohol functionality next to the double bond. πH-bonded complexes of water (W) or the water dimer (W_2) with ethene (Eth), propene (Prop), or allyl alcohol (AOH) were studied in terms of local bond orbital interactions.[6] This study explores further the energetics and electron density redistributions associated with cooperative πH and σH bonds in these complexes and describes the contribution of both σH and πH bonds to the conformational preferences of sphingolipids. The energetic analysis allows us to estimate the nonadditivity of intermolecular interactions, whereas the topological analysis of the electron density gives deeper insight into the properties of OH···π and OH···O interactions.

2. Computational Methods

Optimized geometries for all complexes and isolated monomers were obtained by ab initio Möller−Plesset second-order perturbation theory (MP2) calculations with the frozen core (FC) approximation using the Gaussian 98 electronic structure package.[14] The 6-31+G(d,p) split-valence double-ξ basis set with polarization functions on all atoms and diffuse orbitals on heavy atoms was employed for ceramide and dihydroceramide models (CerM and DHCerM) and the W_2···CerM complex. For the other smaller complexes and isolated monomers, the split-valence, triple-ξ 6-311++G(2d,2p) basis set with a double set of diffuse and polarization functions on all atoms was used. The rationale for using this basis set and level of theory was given in our previous paper.[6] The smaller basis set was employed for larger molecules as a reasonable compromise between quality and feasibility of such calculations. This choice

* To whom correspondence should be addressed. Phone: +1-502-852-5976. Fax: +1-502-852-8149. E-mail: d.dupre@louisville.edu.

10.1021/jp0264580 CCC: $22.00
Published on Web 10/16/2002

is justified by comparable results obtained at both computational levels for the W_2···AOH complex. All optimized geometries were identified as local minima by the absence of imaginary normal-mode frequencies.

The supermolecule approach was used to study energetics of H-bonding interactions in these complexes. Interaction or binding energies (BE), defined as the difference between energy of the complex and that of the isolated monomers (in fully relaxed geometries), were calculated at both Hartree−Fock (HF) and MP2(FC) levels. The correlation energy is defined as the difference between MP2 and HF binding energies. In a few cases, BEs were calculated at the coupled cluster level with single, double, and noniterative triple excitations, CCSD(T).[15] Basis set superposition error (BSSE) was corrected a posteori by the counterpoise (CP) method of Boys and Bernardi.[16] Because of possible overestimation of this correction for correlated methods,[17] values of BSSE are reported here also. The zero-point vibrational energy (ZPVE) difference between a complex and its isolated monomers was also taken into account. CP corrected enthalpy changes for cluster formation, ΔH_{cp}, at 298 K were also calculated.

For any *n*-fragment system, the BE can be partitioned into one-, two-, ..., *n*-body terms.[18] The sum of one-body terms is the total distortion (or relaxation) energy (E_{dist}), which is a quantitative measure of the strain that results from the distortion of the monomer geometry upon the formation of the molecular cluster.[18] The additive part of the BE, ΔE^{2b}, is the pairwise sum of the two-body terms. For trimers, the nonadditive contribution to the BE is represented by the three-body term, ΔE^{3b}, which thus can be used as a measure of cooperative effects.

Natural bond orbital (NBO) theory is useful in understanding molecular complex formation from the point of view of local orbital interactions. The analysis transforms canonical multicenter molecular orbitals into an orthonormal set of one- and two-center localized orbitals (NBOs) analogous to traditional Lewis-type core, bonding (σ and π) and lone pair (n) orbitals, as well as sparsely occupied antibonding (σ^* and π^*) and Rydberg orbitals.[19] In this approach, H-bond formation can be viewed as a result of charge transfer from lone pair or bonding orbitals of the acceptor into antibonding orbitals of the H-bond donor. The energetic stabilization due to CT interactions was estimated here by second-order perturbation analysis and is denoted as $E^{(2)}$.[19] In the framework of NBO theory, atomic charges are determined by natural population analysis (NPA).[19] Natural steric analysis (NSA) provides a numerical estimate of steric exchange repulsions.[20] These calculations were performed using the Gaussian 98 implementation of the NBO 4.0 program[21] with the B3LYP hybrid functional and the same basis set as was used for MP2 geometry optimization.

A more thorough topological analysis of the electron density was performed using Bader's theory of atoms in molecules (AIM).[22] AIM analysis has been applied to study properties of a variety of H-bonded systems exhibiting both conventional and nonconventional H bonds.[23] In particular, the topology of the electron density was analyzed in complexes of π systems (ethene, acetylene, benzene, and more complex ones) with water,[24] hydrogen fluoride, and hydrogen chloride,[25−27] as well as some C−H donors (methane, chloroform, HCN).[24,28] The cooperative enhancement of inter- and intramolecular H-bonding interactions in a variety of molecular clusters has been described using the AIM approach.[29−34] The combination AIM and NBO methodologies used in this work was also proven to be useful in the recent analysis of CH···O hydrogen bonding interactions by Sosa et al.[35]

Morphy98[36] and AIM2000[37] programs were used for the AIM analysis of the electron density from MP2(Full)/6-311++G-(2d,2p) calculations employing Cartesian-type d and f functions in the basis set, as well as density = current and SCF = tight Gaussian keywords. AIM partitions a molecular system into its atomic fragments separated by interatomic surfaces (IAS) of zero-flux in the gradient vector field (GVF) of the electron density ρ.[22] The integration over resultant atomic basins (of volume denoted by Ω) provides values of various properties of individual atoms. The atomic charge, $q(\Omega)$, total energy of the atom, $E(\Omega)$, atomic volume, $\nu(\Omega)$, and dipolar polarization, $\mu(\Omega)$, are among the parameters most relevant to the current study. Atomic integrations are very computationally expensive, especially at the MP2 level.[36] Therefore, all atoms were integrated only in W_2, W···Eth, W_2···Eth, W_2···AOH clusters, and corresponding monomers. Only atomic integration of hydrogen atoms involved in H bonding was performed in other complexes. The accuracy of integration was assessed by the magnitude of a function of the Laplacian of the charge density $L(\Omega)$ defined as $-(1/4)\int_\Omega \nabla^2\rho \, d\tau$, which should be zero for the perfect integration.[22]

The topological analysis of the electron density can be accomplished by finding critical points where $\nabla\rho$, the gradient of ρ, vanishes. The existence, nature, and strength of intermolecular interactions can be assessed by the analysis of the bond critical points (BCP) formed between two interacting atoms.[22] A pair of unique gradient paths, originating at the BCP and terminating at neighboring nuclei, defines a bond path. A molecular graph (MG) is a network of bond paths. For cyclic and cage-type structures, ring (RCP) and cage (CCP) critical points are formed, guaranteeing consistent topology.[22] The Laplacian of ρ, $\nabla^2\rho$, is defined as a sum of eigenvalues (λ_1, λ_2, and λ_3) of the Hessian matrix of the electron density. The topology of $\nabla^2\rho$ reveals regions of local charge concentration and depletion and thus can be used to further characterize H bonds.[22,38] All quantities derived from AIM analysis are given in atomic units (au).

3. Results and Discussion

The possibility of OH···π bond formation in the complex formed between the water dimer and a model molecule that simulates the Cer interface will be discussed first. Energetic and topological analyses of smaller πH-bonded clusters performed at a higher computational level then will be presented.

3.A. πH Bonding in the Interfacial Region of Ceramide. (2*S*,3*R*,4*E*)-2-(*N*-Formylamino)-4-pentene-1,3-diol (denoted CerM) is the smallest molecule that contains all functionalities present in the interfacial region of Cer. Its analogue, lacking the C4═C5 double bond, is denoted DHCerM. To our knowledge, these are the largest ab initio optimized models of the Cer interface yet reported. The optimized complex of CerM with the water dimer, W_2···CerM, is shown in Figure 1. For isolated monomers, the starting orientations of O1−C1−C2−C3 and C1−C2−C3−C4 dihedral angles, (−)syn-clinal in both cases, represent the most populated staggered Cer and DHCer rotamers inferred from NMR spectroscopic observations.[3] For CerM, the orientation of O2−C3−C4−C5 and H−O2−C3−C4 dihedrals, (+)anti-clinal and (−)syn-clinal, respectively, were chosen to be the same as for the most stable conformer of allyl alcohol.[39] The most important geometric parameters for CerM, DHCerM, and the W_2···CerM complex are given in Table S1 of the Supporting Information.

Two intramolecular H bonds, N−H···O1 and O1−H···O2, are formed in these conformations of both CerM and DHCerM.

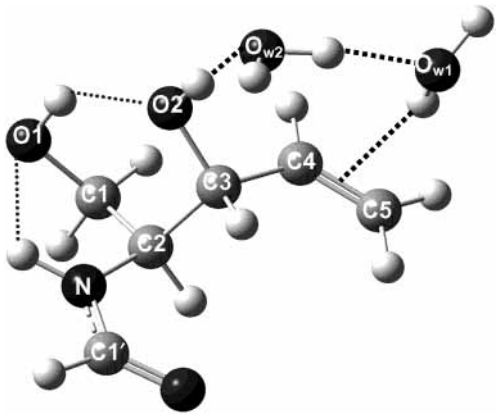

Figure 1. Minimum energy structure for the complex of the water dimer with (2*S*,3*R*,4*E*)-2-(*N*-formylamino)-4-pentene-1,3-diol used as a model for the interfacial region of ceramide. Both intra- and intermolecular H bonds are indicated by dotted lines, which are thinner for intramolecular interactions. Notice that one of the water molecules is tethered by the C4═C5 double bond through OH···π bonding.

For the stronger O1−H···O2 interaction, values for r(H···O2) and ∠(O1−H···O2) are comparable for CerM (1.998 Å, 132.5°) and DHCerM (1.995 Å, 131.5°). These results are not consistent with the strengthening of the intramolecular H-bonding of ceramide due to allylic resonance stabilization, which has also been proposed[40] as a possible mechanism for differences in biochemical behavior of Cer relative to DHCer.

The W_2···CerM complex was optimized from the initial arrangement with one water molecule (w1) placed in the vicinity of the double bond and the other one (w2) H-bonded to both w1 and the allylic alcohol functionality (see Figure 1). This is just one of many possible arrangements for bound water in the interfacial region of Cer. The proposed configuration is, however, plausible because the optimized geometry of this complex is a local minimum, and the ZPVE corrected binding energy of the water dimer to CerM in this complex (−7.06 kcal/mol) is comparable to that in the water trimer (−6.38 kcal/mol). An OH···π and two OH···O intermolecular H bonds occur in the W_2···CerM cluster. The πH-bond distance (from the bound H atom to the center of mass of the double bond) in this complex (2.393 Å) is smaller than that in W···Eth (2.434 Å) and comparable to that in W_2···AOH (2.390 Å) optimized at the same computational level. The OH···π interaction in the W_2···CerM cluster exhibits characteristic properties of H bonds: lengthening of the O−H bond by 0.007 Å and the red shift in the symmetric and asymmetric stretching frequencies by 82 and 55 cm^{-1}, respectively, for the πH-bound water molecule relative to the isolated one. The intermolecular OH···O interaction between the two water molecules is enhanced with respect to the isolated water dimer as evidenced by the decrease in r(H···O) by 0.115 Å. Both intramolecular H bonds are strengthened in the W_2···CerM complex with respect to CerM itself. For instance, the H···O2 distance is decreased by 0.052 Å, the corresponding ∠(O1−H···O2) is increased by 3.0°, the O−H bond is lengthened by 0.002 Å, and ν(OH) is red-shifted by 39 cm^{-1}.

Our calculations thus confirm the possibility for the formation of a cooperative network of σH and πH bonds in the interfacial region of Cer. The presence of water molecules in the vicinity of C4═C5 of Cer results in the extension of its interfacial region as compared to that of DHCer. This arrangement is certainly not static, as water molecules are able to move in and out of the vicinity of the double bond. Saturation of the C4═C5 double bond results in the breakdown of such a network and removal of water from this region. Such conformational differences may contribute to the different signaling behavior of Cer and DHCer.

TABLE 1: Binding Energies[a]

X	ΔE_{cp}	% correl.	BSSE	E_{dist}	ΔZPVE	ΔE_0	ΔH_{cp}
			X···W → X + W				
ethylene	−2.27	71.0	0.57	0.01	1.27	−1.00	−0.90
propene	−2.93	75.4	0.80	0.03	1.30	−1.63	−1.58
allyl OH	−5.46	56.8	1.35	0.26	1.98	−3.48	−3.88
water	−4.45	28.4	0.91	0.04	2.21	−2.24	−2.76
			X···W_2 → X + W_2[b]				
ethylene	−3.80	72.1	0.86	0.25	1.46	−2.34	−2.37
propene	−4.54	73.4	1.13	0.25	1.41	−3.13	−3.12
allyl OH	−7.77	55.0	1.90	1.35	2.06	−5.71	−6.15
water	−9.46	35.2	1.67	1.12	3.32	−6.13	−7.42

[a] All energies are in kcal/mol. W is the water molecule. ΔE_{cp} is the counterpoise corrected binding energy. BSSE is basis set superposition error. Percentage of correlation energy, % correl., is determined from the difference between MP2 and HF binding energies (not corrected for BSSE). E_{dist} is the total distortion energy. ΔZPVE is the zero-point vibrational energy difference. ΔE_0 is ΔE_{cp} corrected for ZPVE. ΔH_{cp} is the counterpoise corrected enthalpy change for complex formation at 298 K. [b] The water dimer (W_2) is considered as a single unit.

3.B. πH Bonding in Smaller Model Systems. Energetic and topological analyses of H-bonding interactions were performed at a higher computational level for the smaller systems used in our previous study,[6] i.e., complexes of water (W) and the water dimer (W_2) with ethene (Eth), propene (Prop), and allyl alcohol (AOH). The cyclic water trimer (W_3) was used to compare the cooperative effects in the πH-bonded complexes with those where only σH bonds are formed. The global minimum structure for the W_3 cluster found in previous studies[29,41] was used as an initial geometry for our optimization. In this cluster, each water molecule acts as a single proton donor and acceptor with two nonbonded H atoms lying above and one below the plane of oxygen atoms. All complexes used in this study are shown in Figure S2, and the most important geometric parameters are given in Table S2 of the Supporting Information. The energetic analysis of binding in these complexes, with emphasis on the cooperative effects, will be discussed first.

3.B.1. Energetic Analysis. Binding energies for dissociation of water from W···Eth, W···Prop, and W···AOH dimers and dissociation of the water dimer from W_2···Eth, W_2···Prop, W_2···AOH, and W_3 trimers are presented in Table 1. W_2 in all trimers was treated as a single unit. Electron correlation comprises a substantial fraction of the uncorrected MP2 BE for all πH-bonded complexes but is much smaller for water clusters (see Table 1). The greater significance of dispersion forces (described only at correlated levels) upon πH-bond formation compared to that for σH bonds was also emphasized in recent studies on W···Eth and W_2···Eth complexes using symmetry adapted perturbation theory (SAPT).[8] Binding energies (in absolute value) increase upon the addition of a second water molecule and/or alcohol functionality (see Table 1). This increase may be traced to the presence of new intermolecular interactions as well as strengthening of existing πH and σH bonding. For the W_2···AOH complex, the CP corrected enthalpy change at 298 K is comparable to that for the water trimer (see Table 1) and is much larger than kT. This confirms that the proposed arrangement is inherently stable at ambient temperature.

Energies for the dissociation of W_2···Eth, W_2···Prop, W_2···AOH, and W_3 trimers into isolated monomers along with their decomposition into n-body terms are given in Table 2. For all of these clusters, there is a substantial difference in total binding energies calculated at MP2 and HF levels. The

TABLE 2: Decomposition of Binding Energies for X···W_2 Trimers[a]

		W_2···Eth	W_2···Prop	W_2···AOH	W_3
ΔE_{cp}	**MP2**	**−8.25**	**−8.94**	**−12.09**	**−13.95**
	HF	−4.56	−4.64	−7.18	−10.09
BSSE	**MP2**	**1.77**	**2.09**	**2.93**	**2.54**
	HF	0.58	0.71	1.01	0.96
E_{dist}	**MP2**	**0.12**	**0.15**	**1.18**	**0.37**
	HF	0.57	0.67	1.34	1.05
ΔE^{2b}	**MP2**	**−7.59**	**−8.15**	**−11.46**	**−12.01**
	HF	−4.28	−4.29	−6.69	−8.83
ΔE^{3b}	**MP2**	**−0.78**	**−0.95**	**−1.81**	**−2.32**
	HF	−0.85	−1.01	−1.83	−2.31

[a] All energies are in kcal/mol. W is water, Eth is ethene, Prop is propene, and AOH is allyl alcohol. ΔE_{cp} is the counterpoise corrected binding energy. BSSE is basis set superposition error. E_{dist} is the total distortion energy (one-body term). ΔE^{2b} and ΔE^{3b} are two- and three-body terms of ΔE_{cp}, respectively.

decomposition of binding energies reveals that the effect of electron correlation is largely concentrated in the additive two-body component (see Table 2). The nonadditive three-body term is always negative and comprises 9.5−16.6% of the CP corrected binding energies at MP2 and 18.6−25.5% of ΔE_{cp} at the HF level. The substantial fraction of the ΔE^{3b} component of BE is in line with cooperative strengthening of H-bonding interactions in these complexes, revealed in the analysis of structural and vibrational parameters in our previous paper.[6] Contrary to the total binding energy or its two-body component, values of ΔE^{3b} are similar at both HF and MP2 levels (see Table 2). Three-body terms calculated at the CCSD(T) level with the same basis set for W_2···Eth and W_3 clusters (−0.74 and −2.28 kcal/mol, respectively) are also similar to Hartree−Fock estimates (see Table 2). Therefore, the match is not due to an inadequate treatment of electron correlation at the MP2 level. The similarity between MP2 and HF three-body terms was also found in the analysis of binding energies for other H-bonded clusters including water trimers.[42,43] These findings are supported by the negligible contribution of three-body dispersion and dispersion-induction energies to the BE in small water clusters found in the recent SAPT analysis by Milet et al.[44]

3.B.2. Natural Bond Orbital Analysis of Donor−Acceptor Interactions. The origin of the cooperative enhancement of πH and σH bonding can be further explored by NBO analysis. Whereas a σH-bonding interaction, such as OH···O, is viewed by NBO theory as a consequence of n(O) → σ*(O−H) electron delocalization, the formation of the πH bond can be considered to be a result of CT from the π-bonding orbital of the C═C double bond, π(C═C), into the antibonding σ*(O−H) orbital of the water molecule, i.e., π(C═C) → σ*(O−H). σH and πH interactions are thus qualitatively the same, differing only in the symmetry of the electron donor orbital and the degree of its overlap with the antibonding orbital of the proton donor.

NBO analysis of stabilizing CT interactions discussed in our previous paper[6] is complemented here by the examination of unfavorable steric exchange interactions. Besides additional energetic stabilization (discussed above), the mutual strengthening of both OH···π and OH···O interactions in trimers manifests itself in the decrease of corresponding H-bonding distances H···|| (where || is the center of mass of the double bond) and H···O (see Tables 3 and 4). This can be viewed as a consequence of the intermolecular CT enhancement, which overcomes unfavorable exchange repulsion interactions between monomers. $E^{(2)}$ estimates for both n(O) → σ*(O−H) and π(C═C) → σ*(O−H) intermolecular delocalizations clearly demonstrate such increases. Unfavorable steric exchange interactions are also

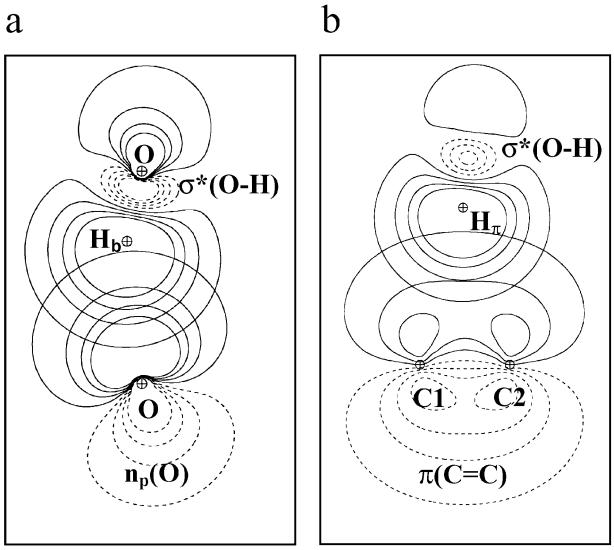

Figure 2. Contour plots of the overlap of preorthogonalized natural bond orbitals (pre-NBOs): oxygen p-type lone pair n_p(O) (a) and π-type bonding orbital π(C═C) (b) with OH antibonding orbitals σ*(OH) in the complex of ethylene with the water dimer. B3LYP/6-311++G(2d,2p)//MP2(FC)/6-311++G(2d,2p) calculations. Nuclear positions are indicated by circled crosses. The outermost contours are at 0.032 au and the contour interval is 0.05 au.

enhanced in complexes of π systems with the water dimer. For instance, pairwise steric exchange energies (provided by NSA) for interactions between π(C═C) or n_p(O) orbitals with σ(O−H) are increased in the W_2···Eth cluster by 0.80 and 0.69 kcal/mol, respectively, relative to corresponding values for W···Eth (2.94 kcal/mol) and the water dimer (6.88 kcal/mol).

The spatial overlap of interacting π(C═C) and σ*(O−H) as well as n_p(O) and σ*(O−H) preorthogonalized NBOs in the W_2···Eth complex is shown in Figure 2. The OH···π interaction is associated with weaker and more diffuse orbital overlap. The value of the overlap integral $S(\pi,\sigma^*) = 0.167$ is also smaller than $S(n,\sigma^*) = 0.250$ for OH···O bonding in this cluster. Thus, πH bonding is expected to be less sensitive to the motion of the bound water molecule in the plane of π bond. This makes structural motifs involving OH···π interactions more flexible, which may also account for the preponderance of such contacts in crystal structures.[1]

3.B.3. Topological Analysis of Electron Density. The theory of AIM is another useful tool which can be used to characterize bonding in molecules and molecular clusters. Interatomic interaction manifests itself by the presence of a bond path and corresponding bond critical point between respective atoms in the equilibrium molecular geometry.[22] Properties of the H···π BCPs for all of the smaller πH-bonded complexes of this study are given in Table 3. The H···π bond path of the W···Eth complex, shown in Figure 3a, terminates at the BCP of the C═C bond rather than a nuclear attractor. This signifies a structural instability of the form of a conflict catastrophe.[22] Such topological instabilities were observed in previous studies for complexes of hydrogen halides with ethylene and acetylene and were related to the flatness of the potential energy surface.[25,26] Any small displacement of the nuclei, or a reduction in symmetry, will result in an abrupt structural change in the topology of ρ. In our models, therefore, the presence of a second water molecule, a methyl group substituent, and/or alcohol functionality switches the H···π bond path towards one of the carbon atoms of the double bond. Then, the πH bond path is highly curved in the vicinity of the C═C bond as seen in Figure 3c.

TABLE 3: Geometric, Energetic, and Topological Parameters Associated with the OH···π Interaction[a]

	W···Eth	W···Prop	W···AOH	W_2···Eth	W_2···Prop	W_2···AOH
$r(H_\pi\cdots\|\|)$[b]	2.395	2.343	2.417	2.341	2.272	2.313
$\angle(O-H_\pi\cdots\|\|)$[b]	167.4	159.7	136.6	156.2	167.1	167.0
			$\pi(C{=}C) \rightarrow \sigma^*(O-H)$ Charge Transfer[c]			
$E^{(2)}$, kcal/mol	2.48	2.79	2.14	3.25	4.46	4.27
			Properties of H···π BCP[d]			
ρ_b	0.0119	0.0134	0.0122	0.0134	0.0160	0.0157
$\nabla^2\rho_b$	0.033	0.038	0.035	0.037	0.041	0.041
ϵ	0.589	0.540	0.629	0.619	0.506	0.365
$\lvert\lambda_1\rvert/\lambda_3$	0.220	0.220	0.210	0.225	0.244	0.235
$H_b(\times 10^3)$	1.16	1.15	1.20	1.11	0.75	0.74
$r(H_\pi)$	1.63	1.59	1.68	1.59	1.51	1.51
$r(\pi)$	2.90	2.84	2.89	2.84	2.79	2.88
$\Delta r(H_\pi)$	0.59	0.64	0.62	0.65	0.72	0.71
$\Delta r(\pi)$	1.11	1.16	1.17	1.16	1.25	1.23

[a] W is water, Eth is ethene, Prop is propene, and AOH is allyl alcohol. [b] Distances are in Å, and angles are in degrees. The πH-bonded hydrogen is denoted as H_π. || indicates the center of mass of the double bond. [c] From NBO analysis, B3LYP/6-311++G(2d,2p) calculations on MP2 optimized structures (same basis set). [d] From AIM analysis, MP2(full)/6-311++G(2d,2p) calculations. BCP is a bond critical point. All AIM quantities are given in atomic units. ρ_b is the electron density at the BCP. $\nabla^2\rho_b$ and ϵ are the Laplacian and ellipticity of ρ_b. $\lvert\lambda_1\rvert/\lambda_3$ is the ratio of the largest negative and positive eigenvalues of the Hessian of ρ at the BCP. H_b is the total energy density at the BCP. r and Δr are the bonded radius and van der Waals penetration of the H_π or π bond. All definitions are given in the text.

TABLE 4: Geometric, Energetic, and Topological Parameters Associated with the OH···O Interaction between Two Water Molecules[a]

	W_2	W_2···Eth	W_2···Prop	W_2···AOH	W_3[e]
$r(H_b\cdots O)$[b]	1.958	1.929	1.910	1.847	1.915
$\angle(O-H_b\cdots O)$[b]	171.7	162.0	168.0	163.6	151.5
			$n_p(O) \rightarrow \sigma^*(O-H)$ Charge Transfer[c]		
$E^{(2)}$, kcal/mol	7.07	7.86	8.77	11.43	8.30
			Properties of H···O BCP[d]		
ρ_b	0.0231	0.0250	0.0261	0.0305	0.0264
$\nabla^2\rho_b$	0.082	0.088	0.090	0.102	0.092
ϵ	0.017	0.021	0.041	0.016	0.013
$\lvert\lambda_1\rvert/\lambda_3$	0.213	0.217	0.223	0.232	0.217
$H_b(\times 10^3)$	1.09	0.82	0.63	−0.20	0.54
$r(H_b)$	1.29	1.27	1.25	1.19	1.27
$r(O)$	2.41	2.38	2.36	2.31	2.36
$\Delta r(H_b)$	0.93	0.96	0.98	1.05	1.00
$\Delta r(O)$	1.17	1.18	1.20	1.27	1.19

[a] W is water, Eth is ethene, Prop is propene, AOH is allyl alcohol. [b] Distances are in Å, angles are in degrees. The σH-bonded hydrogen is denoted as H_b. [c] From NBO analysis, B3LYP/6-311++G(2d,2p) calculations. [d] From AIM analysis, MP2(full)/6-311++G(2d,2p) calculations. The same notation as in Table 3 is used. [e] Results for the strongest OH···O interaction in the water trimer are presented only. All definitions are given in the text.

Cyclic systems of bond paths are formed in all complexes of π systems with the water dimer as well as the W_3 cluster, which produces ring critical points with lower values of electron density than any adjacent BCP (see Figure 3 parts b and c).

Figure 4 shows the projection of the W···Eth molecular graph to the plane of the double bond and πH-bonded H atom, along with the contour plot of ρ and the gradient vector field. The IAS passing through the πH bond critical point is relatively flat, which is typical for H-bonding interactions.[45]

Properties of the πH BCPs (see Table 3) place OH···π interactions within the spectrum of values proposed by Koch and Popelier for H bonds with a range of strengths.[45] Values of ρ at these points, ρ_b, lie within 0.002−0.034 au[45] and are about one-half of the values of ρ_b at the BCPs of the OH···O interaction between two water molecules (cf. data in Tables 3 and 4). Good correlation between values of ρ_b and the strength of corresponding intermolecular interactions for related series of complexes has been found.[29,45,46] The cooperative enhancement of OH···π and OH···O bonding is also seen in the increase in values of ρ_b at corresponding BCPs upon addition of the second water molecule and/or alcohol functionality (see Tables 3 and 4). This trend is consistent with the changes in structural parameters as well as cooperative strengthening of intermolecular CT interactions revealed by NBO analysis (see above).

Values of the Laplacian of ρ, $\nabla^2\rho_b$, at corresponding BCPs for both OH···π and OH···O interactions are small and positive (see Tables 3 and 4). This trend is typical for closed-shell interactions accompanied by depletion of electron density between interacting nuclei.[22] The values also lie within the range typical for H bonds (0.02−0.14 au).[45] The ratio of the largest negative and positive eigenvalues of the Hessian of ρ, $\lvert\lambda_1\rvert/\lambda_3$, is less than unity at both σH and πH bond critical points. This reflects the dominant contraction of the electron density toward the atomic basins found in closed-shell interactions.[22] The local statement of the virial theorem at the BCP (in au), $^1/_4\nabla^2\rho_b = 2G_b + V_b$, relates the Laplacian of ρ to the kinetic energy density, G_b (necessarily positive), and the electronic potential energy density, V_b (always negative). For closed-shell interactions, G_b is in local excess.[22] Thus, the values of the total energy density, H_b, defined as $V_b + G_b$,[47] are positive at H···π and most H···O BCPs as seen in the data of Tables 3 and 4. The magnitude of V_b exceeds that of G_b, but not $2G_b$, for stronger OH···O bonding in the W_2···AOH cluster, making H_b negative but keeping $\nabla^2\rho_b$ small and positive as for typical closed-shell interactions.

The ellipticity of ρ at any BCP, ϵ, is defined as $\lambda_1/\lambda_2 - 1$ where λ_1 and λ_2 are two negative eigenvalues ($\lambda_1 < \lambda_2$) of the Hessian of ρ at the BCP. Values of ϵ provide a measure of the extent to which ρ is asymmetrically concentrated perpendicular to the bond path, and thus can be used to determine the directionality of interatomic interactions.[38] Low values of ϵ characterize BCPs corresponding to OH···O interactions (see Table 4), indicating almost perfect cylindrical σ symmetry. On the other hand, relatively large values of ϵ at the H···π bond critical points (see Table 3) imply greater concentration of ρ along one eigenvector direction with respect to the other, similar to that for π bonds. Along with smaller absolute values of λ_1 and λ_2 (data not shown), the high ellipticity of ρ at H···π BCPs also indicates additional floppiness of πH interactions relative to σH ones. Large ellipticities of ρ are also typical for intermolecular BCPs in van der Waals complexes,[48] indicating their similarity with πH bonds.

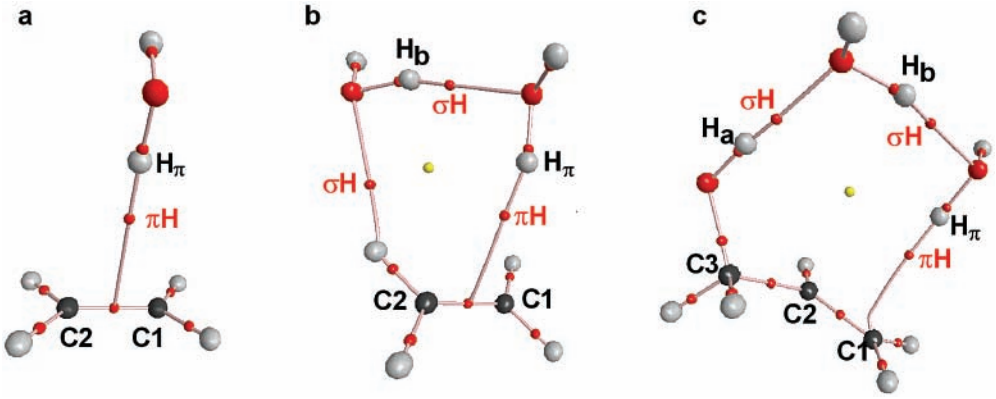

Figure 3. Molecular graphs for some πH-bonded complexes: water···ethylene (a), water dimer···ethylene (b), and water dimer···allyl alcohol (c). Bond paths are denoted by pink cable like connections, nuclei are indicated by large spheres, and bond and ring critical points are denoted by red and yellow small spheres, respectively.

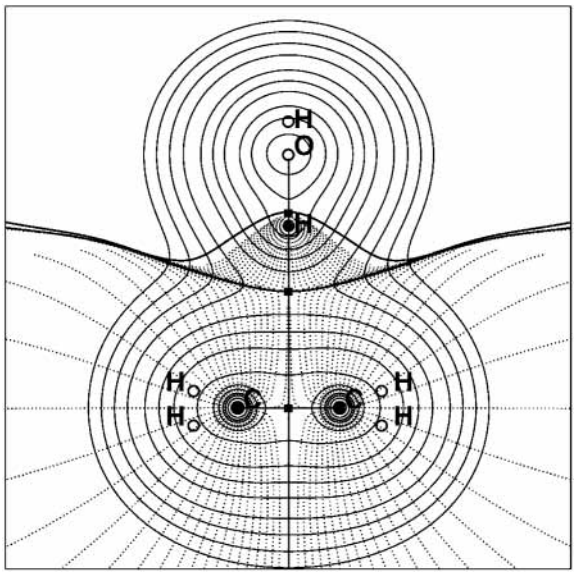

Figure 4. Contour plot of the electron density (solid thin lines) superimposed with the gradient vector field of ρ (dotted thin lines) for the complex of ethylene with water in the plane of the carbon atoms and the πH-bonded hydrogen atom. Projections of bond paths and interatomic surfaces onto this plane are also indicated by thick lines. Bond critical points (BCP) are indicated by solid squares and nuclear positions by solid or open circles for in-plane and out-of-plane nuclei, respectively. The outermost contour of ρ is at 0.001 au, and values of ρ increase as 2×10^n, 4×10^n, and 8×10^n au where $n = -3, -2$, etc. Lines of the gradient vector field are shown only for the atomic basins of in-plane nuclei. The bond path connecting πH-bonded hydrogen atom to the BCP of the C═C bond signifies a topological instability of a conflict catastrophe structure.

Another necessary AIM-based criterion for the intermolecular contact to be considered as a H bond is the mutual penetration of the electron densities of the H atom and acceptor site.[45,46] The acceptor is the oxygen atom for OH···O and the π bond for OH···π interactions. Penetration takes place when the difference between nonbonded (r_0) and bonded (r) radii for both H (Δr_H) and acceptor (Δr_O or Δr_π) atoms is positive.[45,46] The bonded radius is the distance of the nucleus (H or O) or the C═C BCP from the corresponding H···O or H···π BCP in the complex. The nonbonded radius is calculated as the distance from the same nucleus or C═C BCP in the isolated monomer (in the fully relaxed geometry) to a 0.001 au charge density contour in the direction of the πH or σH BCP. The choice of $\rho = 0.001$ au as a practical limit of the molecule gives molecular sizes and atomic diameters in good agreement with gas-phase van der Waals radii.[49] The total penetration (Δr) is the sum of the penetrations for the H atom and the oxygen or π bond. Δr is positive for both OH···O and OH···π interactions (see Tables 3 and 4). Penetration of the H atom upon πH-bond formation is, however, almost twice as small as that for OH···O bonding. This is due to the "softness" of the electron cloud of the π bond relative to that of the oxygen atom. At the same time, both the π bond and the O atom are penetrated to almost equal extent by the H atom of water (cf. Δr_O or Δr_π values in Tables 3 and 4). Such trends are typical for H-bonding interactions.[22] Values of Δr for both types of interaction are also increased in complexes of π systems with the water dimer, which is also a manifestation of cooperative enhancement.

TABLE 5: Integrated Atomic Properties of Hydrogen Atom Participating in OH···π or OH···O Interactions[a]

	$q(\Omega)$	$E(\Omega)$	$\mu(\Omega)$	$\nu(\Omega)$	$L(\Omega)$
W	0.581	−0.370	0.169	22.3	-8.1×10^{-7}
		OH···π (H_π)			
W···Eth	0.587	−0.361	0.162	19.7	-4.5×10^{-5}
W···Prop	0.588	−0.359	0.161	19.0	-3.3×10^{-5}
W···AOH	0.598	−0.353	0.163	19.8	-2.1×10^{-5}
W_2···Eth	0.603	−0.349	0.156	18.3	1.5×10^{-4}
W_2···Prop	0.605	−0.347	0.152	17.4	-3.5×10^{-5}
W_2···AOH	0.606	−0.346	0.152	17.5	-3.3×10^{-5}
		OH···O (H_b)			
W_2	0.622	−0.347	0.133	14.8	-2.9×10^{-5}
W_2···Eth	0.628	−0.342	0.131	14.3	-3.5×10^{-5}
W_2···Prop	0.630	−0.340	0.129	13.9	-3.4×10^{-5}
W_2···AOH	0.645	−0.330	0.122	12.8	-4.1×10^{-5}
W_3	0.640	−0.332	0.128	14.0	-2.5×10^{-5}

[a] W is water, Eth is ethene, Prop is propene, and AOH is allyl alcohol. All integrated properties are given in atomic units. $q(\Omega)$ is the atomic charge, $E(\Omega)$ is energy of the atom, $\mu(\Omega)$ is atomic dipole moment, and $\nu(\Omega)$ is atomic volume. $L(\Omega)$ is defined in the text and used as a measure of the integration accuracy.

Changes in the integrated properties of the H atom participating in OH···O (H_b) and OH···π (H_π) interactions with respect to corresponding monomer values were also evaluated. Selected atomic properties of H_b and H_π are listed in Table 5. An increase in atomic charge, $q(\Omega)$, is observed for both H_b and H_π atoms with respect to a H atom in the isolated water molecule. Such loss of electron density around the H atom is typical in H-bonding interactions.[45,46] Values of $q(\Omega)$ for both H_b and H_π atoms also increase upon addition of a second water molecule and alcohol functionality, being the greatest for the W_2···AOH complex. In this cluster, the loss of charge is almost three times as great for the H atom involved in the OH···O interaction (0.064 au) as that for H_π (0.024 au). These trends are in line

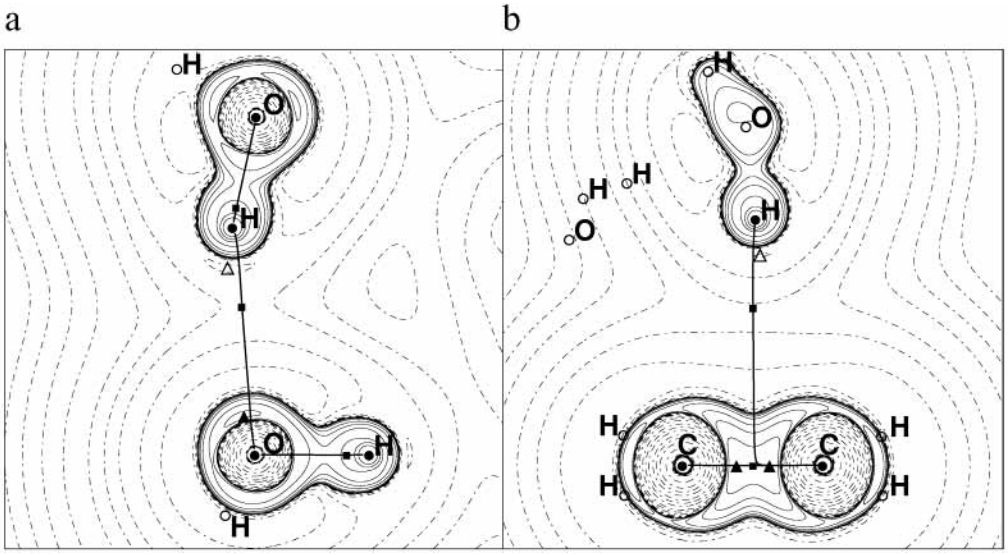

Figure 5. Contour plots of the negative of the Laplacian of the electron density $L(r)$ for the complex of ethylene with the water dimer in the plane of OH···O (a) or OH···π (b) bonded atoms. Solid contours denote positive values of $L(r)$, regions of charge concentration, and dashed contours denote $L(r) < 0$, i.e., regions of charge depletion. Values of $L(r)$ begin at zero and increase or decrease as $\pm 2 \times 10^n$, $\pm 4 \times 10^n$, and $\pm 8 \times 10^n$ au where $n = -3, -2, -1, 0, +1$, and $+2$. Bond paths are shown as solid lines connecting nuclei. Bond critical points are indicated by solid squares and nuclear positions by solid or open circles for in-plane and out-of-plane nuclei, respectively. Maxima and minima in $L(r)$ are denoted by solid and open triangles, respectively.

with an increase in NPA charges for H_b and H_π atoms[6] and greater polarization of the σ(O−H) orbital toward oxygen in these clusters. The increase in $q(\Omega)$ is also accompanied by the energetic destabilization of the bonded H atom: $E(\Omega)$ goes up because of the loss of electrons (see Table 5). This trend is also typical for H-bonding interactions.[45,46] The degree of destabilization parallels the strength of H bonds.[46] Thus, the increase in $E(\Omega)$ is greater for H_b than for H_π atom in πH-bonded clusters. As a consequence of the loss of electron density, the dipolar polarization, $|\mu(\Omega)|$, of the H-bonded atom decreases in these clusters (see Table 5). The atomic dipole moment typically opposes the direction of the charge transfer.[22,38] Thus, the decrease in $|\mu(\Omega)|$ removes electron density from the bonded region facilitating mutual penetration of the H and acceptor atoms.[46] The loss of the dipolar polarization is much greater for the H atom involved in the OH···O interaction because of greater removal of charge caused by the "harder" O atom compared to the "softer" π bond (see Table 5). The atomic volume, $\nu(\Omega)$, of the H-bonded hydrogen atom goes down.[38,46] The decrease in $\nu(\Omega)$ is related to the formation of the new IAS, which results in the removal of the outermost charge density from a H atom.[46] As a result of the stronger and more directional OH···O interaction, the shrinkage is more pronounced for H_b than for H_π (see Table 5).

The electron density redistribution in these clusters can be analyzed by comparison of atomic charges for all atoms in the complex with those in isolated monomers (see Table S3 of the Supporting Information). In terms of AIM-derived charges, the flow of negative charge from the Lewis base (H-bond acceptor) to the acid (H-bond donor) is relatively small, e.g., 0.024e in the W···Eth complex and 0.019e in the water dimer. However, charge redistribution within monomers is much greater and results in a loss of electron density from the tail of the base and a comparable gain of charge by the head of the acid.[46] For instance, in the W···Eth complex, the water O atom gains 0.024e, whereas 0.016e is lost from each H atom of H_2O acting as a base in W_2. Such charge redistribution facilitates further H-bonding capabilities of these atoms. This results in the cooperative enhancement of both OH···O and OH···π interactions in the W_2···Eth complex. In clusters of π systems with the water dimer, the flow of electron density is more complex because of formation of the cyclic network of πH and σH bonds. In the W_2···AOH cluster, the oxygen atom of the allyl alcohol moiety experiences the greatest gain of charge (0.061e) which makes it a better H-bond acceptor. This accounts for the strengthening of the intramolecular OH···O bond, taking place in the W_2···CerM complex (see above). Such trends are in qualitative agreement with results of NPA on these clusters (see Table S4 of the Supporting Information) used in our previous paper.[6] However, the magnitudes of AIM-derived charges, as well as the amount of CT, are usually greater than those derived from orbital based partitioning schemes. When calculating bond dipoles, discrepancies are reduced because opposing dipolar polarization within atomic basins must be included.[22,38]

The topology of the function $L(r)$ defined as the negative of the Laplacian of ρ, $-\nabla^2\rho$,[38] allows further characterization of OH···π and OH···O interactions. In the valence shell (VS) of atoms in molecules, this function is positive for regions of charge concentration (VSCC) and negative for regions of charge depletion (VSCD).[38,50] The contour plots of $L(r)$, along with projections of molecular graphs, for both OH···O and OH···π bonded atoms in W_2···Eth cluster are shown in Figure 5. As typical for closed-shell interactions, regions of VSCC for interacting atoms are separated. H···π and H···O BCPs are located in the VSCD zone (see Figure 5). Local maxima in $L(r)$ within regions of VSCC can be mapped to the bonded and nonbonded (lone) electron pairs of Lewis and VSEPR (valence shell electron pair repulsion) models.[50] Furthermore, structures of H-bonded clusters can be predicted by the alignment of the maximum in $L(r)$ of the Lewis base (H-bond acceptor) with the minimum in $L(r)$ for the Lewis acid (H-bond donor).[38] The OH···O interaction between two water molecules in the W_2···Eth cluster can be viewed as a combination of the nonbonded charge concentration ($L(r) = 4.855$ au, 0.653 au away from the nucleus) of the Lewis base oxygen atom with the electron density depletion ($L(r) = -0.216$ au, 0.649 au away from the nucleus) of the σH-bonded hydrogen atom. The alignment of these critical points in $L(r)$ is reminiscent of the

n(O) and σ^*(O−H) NBO overlap (cf. Figures 2a and 5a). Similarly, the OH···π interaction can be viewed as a result of the combination of the charge depletion (0.650 au away from the nucleus) of the πH-bonded H atom with bonded charge concentrations of the C═C bond. This is reminiscent of the π(C═C) and σ^*(O−H) NBO overlap discussed above (cf. Figures 2b and 5b). There are two bonded maxima in $L(r)$ along the C═C bond of much smaller magnitude (1.266 and 1.271 au) and located further away from the nuclei (∼0.97 au) than the nonbonded oxygen maximum (see above). This accounts for the "softness" of the π bond electron density and additional floppiness of the OH···π interaction with respect to the conventional OH···O bond. Therefore, the displacement of bound water molecule in the plane of the double bond is barely restricted. In the W···Eth complex, the two maxima in the VSCC of the C═C bond are equivalent, accounting for the formation of the conflict catastrophe structure and its breakdown upon reduction of molecular symmetry (see above).

4. Conclusions

This work supports the formation of cooperative πH and σH bonds in the interfacial region of ceramide proposed earlier on the basis of experimental findings.[3] Thus, the trans C4═C5 double bond may serve not only as a kink, restricting flexibility of the molecule, but also as a tethering site of water molecules. The formation of this structural motif is not possible in the saturated ceramide analogue, dihydroceramide. These findings also imply the extension of the interfacial region of ceramide, which affects its packing in the lipid bilayer and accessibility by various molecular agents including proteins involved in signal transduction pathways. This model, therefore, provides a reasonable explanation for the very different signaling properties of ceramide and its saturated analogue.

The OH···π interaction in the complex of ethylene with water is weaker than the OH···O bond in the water dimer. However, both πH and σH bonding are cooperatively enhanced in clusters of the water dimer with π systems and act together in the stabilization of the W_2···AOH complex. OH···π interactions are characterized by a much greater contribution of dispersion forces than conventional H bonds and require application of correlated methods for their description. However, the substantial nonadditive three-body component of the binding energy is adequately described at the Hartree−Fock level. Natural bond orbital theory attributes this nonadditivity to the cooperative charge-transfer interactions among local bond orbitals, which overcomes unfavorable steric exchange repulsions and results in the strengthening of both OH···π and OH···O interactions in complexes of π systems with the water dimer. As revealed by the population analysis, such enhancement results from the electron density flow from the tails of the H-bond acceptor to the head of the donor which makes them more prone to additional H bonding. Qualitatively similar results were obtained using charges derived from both NBO and AIM theories.

The H-bonding nature of the OH···π interaction was confirmed by the topological analysis of the electron density applying the theory of AIM. The cooperative enhancement of both πH and σH bonding in these complexes is manifested in greater accumulation of electron density, mutual penetration, and changes in atomic properties of bonded atoms. These changes are substantially smaller for OH···π interactions, which was attributed to the softness of the electron cloud for π bond compared to that of the oxygen atom. Indeed, the topology of the Laplacian of ρ reveals a smaller and less tightly bound accumulation of the electron density associated with the C═C bond. This is reminiscent of the weaker and more diffuse overlap between π(C═C) bonding and σ^*(O−H) antibonding orbitals revealed by NBO analysis. Thus, both methods predict additional floppiness of πH vs σH bonding: water molecules tethered by the OH···π bond are expected to be more flexible than those bound by the OH···O interaction. This implies a relatively wide range of optimal angles of approach of H_2O or other polar agents to the double bond.

This study demonstrates that both AIM and NBO methods are valuable complementary tools to elucidate the nature of intermolecular interactions in H-bonding networks. AIM provides a very sophisticated analysis of the electron density within a molecular system. NBO helps to understand the most important routes of electron delocalization that produce this density distribution. The results of this study have not only theoretical but also practical importance. They confirm the relevance of the πH bond in the formation of structural motifs that differentiate ceramide from its saturated analogue and may be helpful in the elucidation of structural/functional relationships that contribute to the signaling properties of sphingolipids.

Acknowledgment. We gratefully acknowledge the National Eye Institute of the National Institutes of Health, which has supported this research through Grant EY11657. Computer time allocations were received from the National Computational Science Alliance under Grants CHE98008N and CHE990012N and the Advanced Biomedical Computing Center of the Frederick Cancer Research and Development Center, National Institutes of Health.

Supporting Information Available: Two figures and four tables are given as Supporting Information. This material is available free of charge via the Internet at http://pubs.acs.org.

References and Notes

(1) Desiraju, G. R.; Steiner, T. *The weak hydrogen bond in structural chemistry and biology*; Oxford University Press: New York, 1999.

(2) Subramanian, K.; Lakshmi, S.; Rajagopalan, K.; Koellner, G.; Steiner, T. *J. Mol. Struct.* **1996**, *384*, 121.

(3) Li, L.; Tang, X.; Taylor, K. G.; DuPré, D. B.; Yappert, M. C. *Biophys. J.* **2002**, *82*, 2067.

(4) Ohanian, J.; Ohanian, V. *Cell. Mol. Life Sci.* **2001**, *58*, 2053.

(5) Bielawska, A.; Crane, H.; Liotta, D.; Obeid, L.; Hannun, Y. *J. Biol. Chem.* **1993**, *268*, 26226.

(6) DuPré, D. B.; Yappert, M. C. *J. Phys. Chem. A* **2002**, *106*, 567.

(7) Tarakeshwar, P.; Kim, K. S.; Brutschy, B. *J. Chem. Phys.* **2001**, *114*, 1295.

(8) Kim, K. S.; Tarakeshwar, P.; Lee, J. Y. *Chem. Rev.* **2000**, *100*, 4145.

(9) Aspiala, A.; Lotta, T.; Murto, J.; Rasanen, M. *Chem. Phys. Lett.* **1984**, *112*, 469.

(10) Bjerkeseth, L. H.; Bakke, J. M.; Uggerud, E. *J. Mol. Struct.* **2001**, *567*, 319.

(11) Kowski, K.; Luttke, W.; Rademacher, P. *J. Mol. Struct.* **2001**, *567*−*568*, 231.

(12) Mons, M.; Robertson, E. G.; Snoek, L. C.; Simons, J. P. *Chem. Phys. Lett.* **1999**, *310*, 423.

(13) Rovira, M. C.; Novoa, J. J.; Whangbo, M. H.; Williams, J. M. *Chem. Phys.* **1995**, *200*, 319.

(14) Frisch, M. J.; Trucks, G. W.; Schlegel, H. B.; Scuseria, G. E.; Robb, M. A.; Cheeseman, J. R.; Zakrzewski, V. G.; Montgomery, J. A., Jr.; Stratmann, R. E.; Burant, J. C.; Dapprich, S.; Millam, J. M.; Daniels, A. D.; Kudin, K. N.; Strain, M. C.; Farkas, O.; Tomasi, J.; Barone, V.; Cossi, M.; Cammi, R.; Mennucci, B.; Pomelli, C.; Adamo, C.; Clifford, S.; Ochterski, J.; Petersson, G. A.; Ayala, P. Y.; Cui, Q.; Morokuma, K.; Malick, D. K.; Rabuck, A. D.; Raghavachari, K.; Foresman, J. B.; Cioslowski, J.; Ortiz, J. V.; Stefanov, B. B.; Liu, G.; Liashenko, A.; Piskorz, P.; Komaromi, I.; Gomperts, R.; Martin, R. L.; Fox, D. J.; Keith, T.; Al-Laham, M. A.; Peng, C. Y.; Nanayakkara, A.; Gonzalez, C.; Challacombe, M.; Gill, P. M. W.; Johnson, B. G.; Chen, W.; Wong, M. W.; Andres, J. L.; Head-Gordon, M.; Replogle, E. S.; Pople, J. A. *Gaussian 98*, revision A.9; Gaussian, Inc.: Pittsburgh, PA, 1998.

(15) Urban, M.; Noga, J.; Cole, S. J.; Bartlett, R. J. *J. Chem. Phys.* **1985**, *83*, 4041.

(16) Boys, S. F.; Bernardi, F. *Mol. Phys.* **1970**, *19*, 553.
(17) Cook, D. B.; Sordo, J. A.; Sordo, T. L. *Int. J. Quantum Chem.* **1993**, *48*, 375.
(18) Xantheas, S. S. *J. Chem. Phys.* **1994**, *100*, 7523.
(19) Weinhold, F. Natural Bond Orbital Methods. In *Encyclopedia of computational chemistry*; Schleyer, P. v. R., Allinger, N. L., Clark, T., Gasteiger, J., Kollman, P. A., Schaefer, H. F., III., Schreiner, P. R., Eds.; John Wiley & Sons: Chichester, U.K., 1998; Vol. 3, p 1792.
(20) Badenhoop, J. K.; Weinhold, F. *J. Chem. Phys.* **1997**, *107*, 5406.
(21) Weinhold, F. *NBO 4.M Program Manual*; Theoretical Chemistry Institute: University of Wisconsin, Madison, WI, 1996.
(22) Bader, R. F. W. *Atoms in molecules: a quantum theory*; Clarendon Press: New York, 1990.
(23) Popelier, P. L. A.; Aicken, F. M.; O'Brien, S. E. Atoms in molecules. In *Chemical Modelling: Applications and Theory*; Hinchliffe, A., Ed.; Royal Society of Chemistry: Cambridge, U.K., 2000; Vol. 1, p 506.
(24) Novoa, J. J.; Mota, F. *Chem. Phys. Lett.* **2000**, *318*, 345.
(25) Zhang, Y. H.; Hao, J. K.; Wang, X.; Zhou, W.; Tang, T. H. *J. Mol. Struct. THEOCHEM* **1998**, *455*, 85.
(26) Rozas, I.; Alkorta, I.; Elguero, J. *J. Phys. Chem. A* **1997**, *101*, 9457.
(27) Lin, Z.; Bytheway, I. *Chem. Phys. Lett.* **1995**, *240*, 541.
(28) Cubero, E.; Orozco, M.; Hobza, P.; Luque, F. J. *J. Phys. Chem. A* **1999**, *103*, 6394.
(29) Mo, O.; Yanez, M.; Elguero, J. *J. Chem. Phys.* **1992**, *97*, 6628.
(30) Rincon, L.; Almeida, R.; Garcia-Aldea, D.; Riega, H. D. Y. *J. Chem. Phys.* **2001**, *114*, 5552.
(31) Luque, F. J.; Lopez, J. M.; de la Paz, M. L.; Vicent, C.; Orozco, M. *J. Phys. Chem. A* **1998**, *102*, 6690.
(32) Gonzalez, L.; Mo, O.; Yanez, M. *J. Chem. Phys.* **1999**, *111*, 3855.
(33) Parra, R. D.; Zeng, X. C. *J. Chem. Phys.* **1999**, *110*, 6329.
(34) Masella, M.; Flament, J. P. *J. Chem. Phys.* **1999**, *110*, 7245.
(35) Sosa, G. L.; Peruchena, N. M.; Contreras, R. H.; Castro, E. A. *J. Mol. Struct. THEOCHEM* **2002**, *577*, 219.
(36) Popelier, P. L. A.; Bone, R. G. A. *MORPHY98*; UMIST: Manchester, U.K., 1998.
(37) Biegler-Konig, F.; Schonbohm, J.; Bayles, D. *J. Comput. Chem.* **2001**, *22*, 545.
(38) Popelier, P. L. A. *Atoms in molecules: an introduction*; Prentice Hall: New York, 2000.
(39) Badawi, H.; Lorencak, P.; Hillig, I.; Kurt W.; Imachi, M.; Kuczkowski, R. L. *J. Mol. Struct.* **1987**, *162*, 247.
(40) Simon, C. G., Jr. *Biochemistry* **1998**, *37*, 2059.
(41) Xantheas, S. S.; Dunning, T. H. *J. Chem. Phys.* **1993**, *98*, 8037.
(42) Chalasinski, G.; Szczesniak, M. M.; Cieplak, P.; Scheiner, S. *J. Chem. Phys.* **1991**, *94*, 2873.
(43) Klopper, W.; Schutz, M.; Luthi, H. P.; Leutwyler, S. *J. Chem. Phys.* **1995**, *103*, 1085.
(44) Milet, A.; Moszynski, R.; Wormer, P. E. S.; van der Avoird, A. *J. Phys. Chem. A* **1999**, *103*, 6811.
(45) Koch, U.; Popelier, P. L. A. *J. Phys. Chem.* **1995**, *99*, 9747.
(46) Carroll, M. T.; Bader, R. F. W. *Mol. Phys.* **1988**, *65*, 695.
(47) Cremer, D.; Kraka, E. *Croat. Chem. Acta* **1984**, *57*, 1259.
(48) Bone, R. G. A.; Bader, R. F. W. *J. Phys. Chem.* **1996**, *100*, 10892.
(49) Bader, R. F. W.; Carroll, M. T.; Cheeseman, J. R.; Chang, C. *J. Am. Chem. Soc.* **1987**, *109*, 7968.
(50) Bader, R. F. W.; Gillespie, R. J.; Macdougall, P. J. *J. Am. Chem. Soc.* **1988**, *110*, 7329.